INTERDIFFUSION BEHAVIORS OF U-Mo-Zr/Al-Si

Jong Man Park, Ho Jin Ryu, Seok Jin Oh, Don Bae Lee, Chang Kyu Kim
Korea Atomic Energy Research Institute, 150 Deokjin-dong, Yuseong-gu, Daejeon 305-353, Korea

and

Yeon Soo Kim, G. L. Hofman
Argonne National Laboratory, 9700 S. Cass Ave, Argonne, IL 60439, USA

ABSTRACT

We investigated the effect of a Zr addition to U-Mo on the reaction between U-Mo-Zr and Al-Si by out-of-pile tests, dispersion annealing and diffusion couple tests. By using vacuum induction melting and centrifugal atomization techniques, ingots and powders of U-7wt.%Mo alloys with 1, 2 and 4 wt.% Zr were fabricated. We examined the gamma phase stability of the gamma-heat-treated alloys by high-temperature annealing tests. Using the X-ray diffraction method, we observed that the gamma phase U-7Mo-Zr alloys decomposed similar to the U-7Mo alloys. To examine the inter-diffusion behavior, we fabricated dispersion samples by using U-Mo-Zr powders and Al-(0, 0.4, 2, 5)wt.%Si alloys. To compare the interdiffusion behaviors between annealing tests of the dispersion samples and diffusion couple samples, we prepared diffusion couples with the same compositional combinations as the dispersion samples and tested. Dispersion samples with high Zr contents slightly increased the inter-diffusion rates at 600°C, whereas the diffusion couples showed that a Zr addition to U-7Mo reduced the interaction rates. We were able to confirm the Si effect of suppressing the interaction growth rates. Zr added to U-Mo did not accumulate in the interaction layers to a large extent, whereas Si did when added to Al. An interaction product with the composition of Si-rich $U(Si,Al)_2$ was formed on U-Mo-Zr in a U-Mo-Zr vs. Al-Si diffusion couple.

1. Introduction

U-Mo alloy dispersion fuel is being developed as a high uranium density fuel for high performance research reactors due to its excellent stability during an irradiation [1]. However, an unacceptable volume expansion due to an interaction layer (IL) formation and a subsequent gross pore formation at the interface between U-Mo and matrix Al has hampered its further development [2]. Based upon the diffusion couple test data that a Si addition to Al has a beneficial effect in reducing the reaction rate [3] and from a metallurgical study that a Si accumulation in the reaction product improves its stability [4], ANL has proposed an Al-matrix modification by adding Si as a remedy to tackle the problem in U-Mo/Al dispersion fuel [4]. Previous out-of-pile diffusion studies showed that Si accumulates into the IL in U-Mo/Al-Si dispersion fuel samples [5,6]. U-Mo/Al-Si dispersion fuel in the irradiation test plates showed a considerable reduction with regard to their plate volume expansion from the plates using pure Al as the matrix [7,8]. Irradiation tests with rod-type fuel elements containing U-Mo/Al-Si dispersion fuel are under way [9].

Zirconium was identified as another element for stabilizing the IL (i.e., UAl_3) in the previous study [10]. Because of potential reprocessing difficulties of the spent fuel containing a high-Si content and in

the hope of improving the stability of the reaction product further, Zr addition to U-Mo was also proposed [4]. Since atomistic simulations of U-Mo-Zr vs. Al-Si diffusion couples showed auspicious results, out-of-pile tests have been adapted to confirm the effects of Zr before irradiation tests.

This paper presents the results from diffusion-couple tests and dispersion annealing tests between U-Mo-xZr and Al-ySi, namely, U-Mo/Al, U-Mo-Zr/Al, U-Mo/Al-Si, and U-Mo-Zr/Al-Si with various contents of Zr and Si. The results revealed that both the Zr addition to U-7wt%Mo and the Si addition to Al, either in combination or separately, suppressed the growth of the ILs. The Si accumulation in the ILs was enhanced by the Zr addition to U-Mo. We noticed that the interaction product of a U-Mo-Zr vs. Al-Si diffusion couple test is comprised of two layers, where the layer on U-Mo side was composed of an interaction product with an approximate composition of $U(Si,Al)_2$, with an Si/Al ratio greater than one.

2. Experimental Procedures

For the diffusion couple tests, we fabricated U-7wt%Mo-xZr (x=0, 1, 2, 4 wt%) alloys by using a vacuum-induction melting in a zirconia crucible. The as-cast U-7Mo-xZr ingots were then heat-treated in a vacuum at 950°C for 24 hr and sequentially water-quenched to stabilize the γ-U phase. Stabilities of the γ-phase of the U-Mo-xZr alloys were compared by using X-ray diffraction (XRD) after an annealing at 500°C from 10 min to 48 hr. The U-Mo-Zr vs. Al-Si diffusion couples were also annealed at 580°C and 600°C from 1 to 10 hr in a vacuum-sealed quartz tube.

For the dispersion-fuel annealing tests, we fabricated U-7Mo-xZr (x=0, 1, 2, 4 wt%) powders by the centrifugal atomization method. Spherical particles within the size range of 150-210 μm were selected. The U-7Mo-xZr powders and Al-ySi (y=0, 0,4, 2, 5 wt%) powders were blended and hot-extruded at 400°C to fabricate dispersion samples with a 10 vol.% particle loading. The dispersion samples were annealed at 550~600°C for up to 50 hr in a vacuum atmosphere.

Microstructures of the interaction layers (ILs) in the diffusion-couple-test specimens and the annealed dispersion fuel samples were observed by using a scanning electron microscopy (SEM). Concentration profiles of the ILs in the diffusion couples and in the annealed dispersion fuel samples were measured by using a microprobe equipped with an energy dispersive spectrometer, i.e., an electron probe micro-analysis (EPMA).

3. Results and Discussion

3-1. Gamma Phase Stability

The γ-phase U-7Mo-xZr alloys annealed at 500°C transformed to a mixture of the α-U phase and the γ′-U_2Mo phase because the γ-phase is instable below ~600°C for a U-7Mo alloy. Figure 1 compares the effects of a Zr addition on the stability of the γ-phase of the U-7Mo-xZr ternary alloys. Even after 10 min of an annealing at 500°C, the U-7Mo-xZr alloys shows virtually the same diffraction patterns as the transformed U-Mo alloys as shown in Fig. 1(a). The effect of a Zr addition for these tests, annealed at 500°C for 10 min, is nill in the XRD patterns. This means that the γ-phase U-7Mo decomposes at this temperature so fast that a Zr addition does not influence the rate. It is known that the effect of a Zr addition on the γ-phase U-Mo is to decrease the γ-phase stability of U-Mo alloys [11,12]. This was observed for a longer annealing test as shown in Fig.1(b). We can see distinct diffraction peaks for the (103) planes of the γ′-phase in the U-7Mo-2Zr and U-7Mo-4Zr samples annealed for 16 hr as shown in Fig. 1(b). This result confirms that a Zr addition to U-7Mo generally reduces the γ-phase stability and

the transformation rate increases as the Zr content increases. The SEM images of the decomposed γ-phase after an annealing test(48 hr) are shown in Fig. 2. The transformed microstructures of U-7Mo-2Zr and U-7Mo-4Zr are too fine to identify their phase evolution.

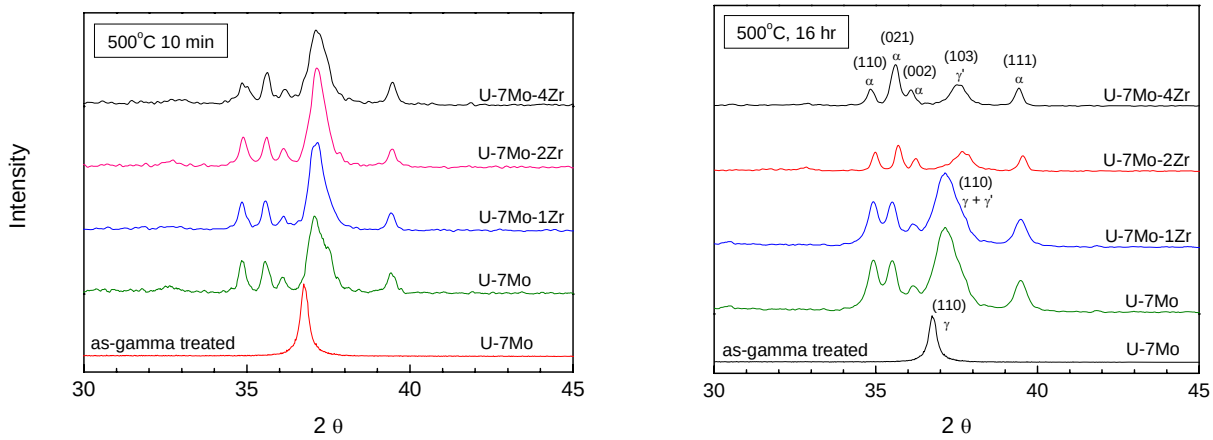

(a) (b)

Fig. 1. X-ray diffraction patterns showing the transformation of the γ-phase in the U-7Mo-xZr annealed at 500°C (a) for 10 min and (b) for 16 hr.

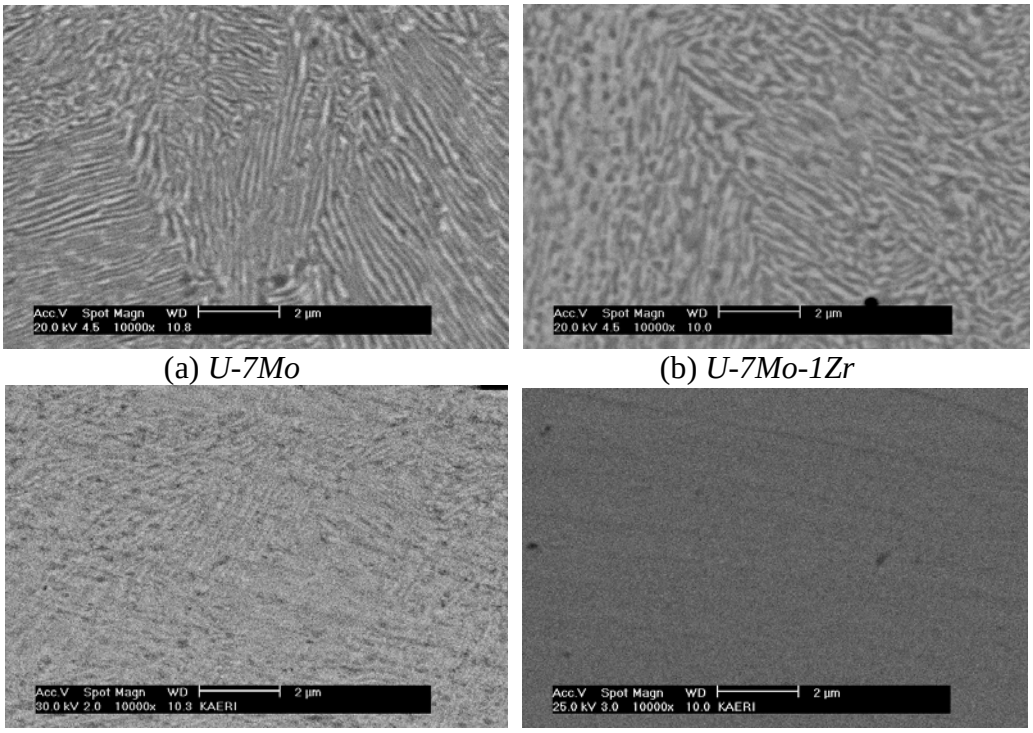

(a) *U-7Mo* (b) *U-7Mo-1Zr*

(c) *U-7Mo-2Zr* (d) *U-7Mo-4Zr*

Fig. 2. SEM images of the U-7Mo-xZr after an annealing at 500°C for 48 hr.

3-2. Microstructural Analysis and Growth of the Interaction Layers

Atomized particles of U-Mo alloy have a metastable cellular structure due to a rapid solidification. It is known that the Mo content is lower, by about 2~3 at.%Mo, at the cell boundaries compared to the overall content [13]. Atomized U-Mo-Zr alloys also form similar cellular structures. As shown in Fig. 3, a metallographic etching revealed the cell boundaries as well as the grain boundaries in an atomized particle. The grain boundaries have darker lines and are more widely spread than the cell boundaries.

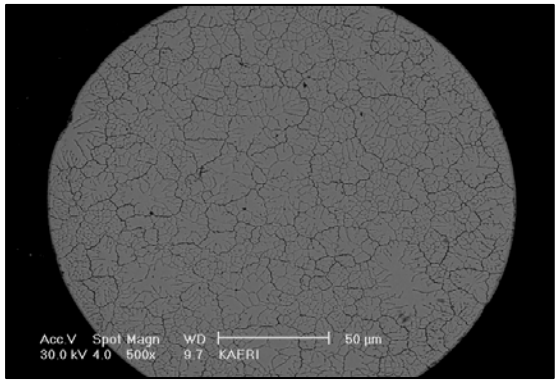

Fig. 3. SEM images of a U-7Mo-1Zr alloy particle in a dispersion fuel sample after a metallographic etching.

Figures 4~6 display some examples of the ILs formed in the U-Mo-Zr/Al-Si dispersion fuel samples after an annealing at 550 or 600°C. As can be seen in Fig. 4, Zr addition to U-Mo results in an enhanced inter-diffusion of Al along the cell boundaries. There are many possible reasons for this: (i) the α-phase has higher diffusivities for Al diffusion than the γ-phase. (ii) Because the cell boundaries have lower Mo concentrations than in the cell, resistance to Al diffusion by Mo is lower than in the cell. (iii) Zr may facilitate the Al diffusion in the cell boundaries. The dark phase along the cell boundaries has the same composition as the IL between the U-Mo particles and Al matrix as shown in the X-ray elemental map of Fig. 5.

The inter-diffusion between U-Mo-Zr and Al-Si yields the most complicated microstructures. Figure 6 compares the microstructures of the U-Mo/Al-Si and U-Mo-Zr/Al-Si dispersion samples annealed at 600°C for 3 hr. The remarkable difference is in the cell size: the cell size in the U-Mo-Zr/Al-Si sample is much smaller than U-Mo/Al-Si. The cells are depicted with interaction phases along their boundaries. The IL thickness of U-Mo-Zr/Al-Si is slightly thinner than that of U-Mo/Al-Si. As will be discussed later, however, comparing the IL growth rates from the dispersion sample tests provides meaningless results mainly because the interaction products from these data are irregular, making a thickness measurement impossible.

In Fig. 7, X-ray elemental maps of a U-7Mo-2Zr/Al-5Si dispersion sample reveal the distributions of U, Mo, Zr, Al and Si in the fuel and IL after an annealing. The most notable feature is the distribution of Si in the fuel particle. It is also distributed uniformly in the IL and found as precipitates in the Al matrix. On the contrary, Zr is distributed fairly uniformly in the fuel and accumulates slightly in the IL, suggesting that a Zr accumulation in the IL at this temperature is much less active than that of Si. This characteristic was consistent with the findings reported in Ref. 6 and will be discussed in more detail later.

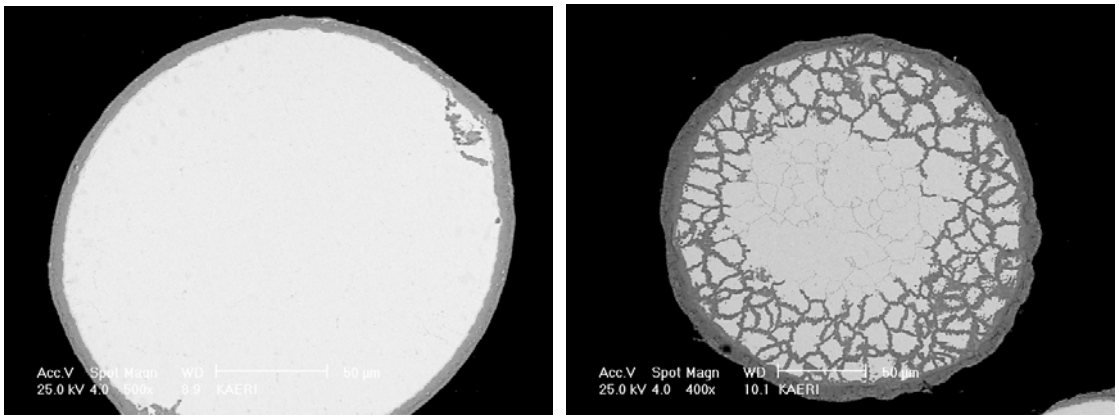

(a) (b)

Fig. 4. SEM images of the dispersion samples after an annealing at 600°C for 1 hr;(a) U-7Mo/Al dispersion and (b) U-7Mo-4Zr/Al dispersion. The reaction products along the cell boundaries are shown in gray.

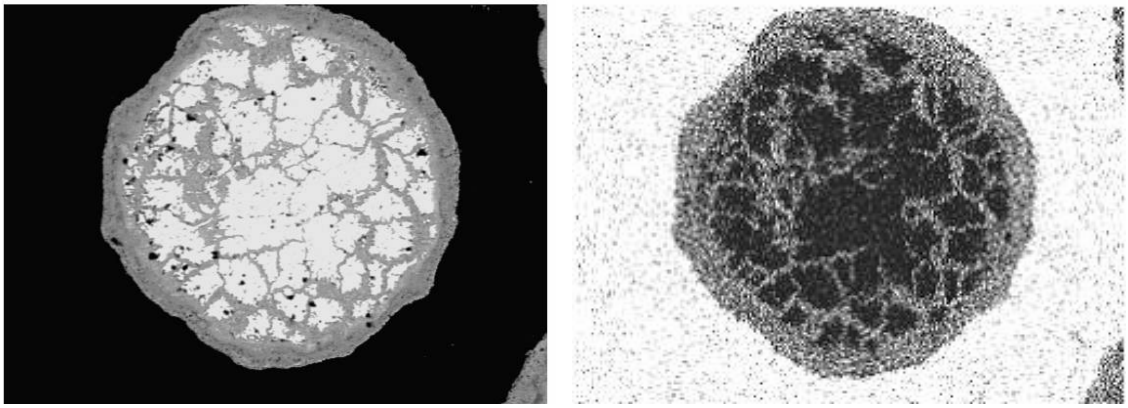

(a) (b)

Fig. 5. (a) SEM image and (b) X-ray elemental map for the Al of the U-7Mo-4Zr/Al dispersion fuel sample annealed at 600°C for 1 hr.

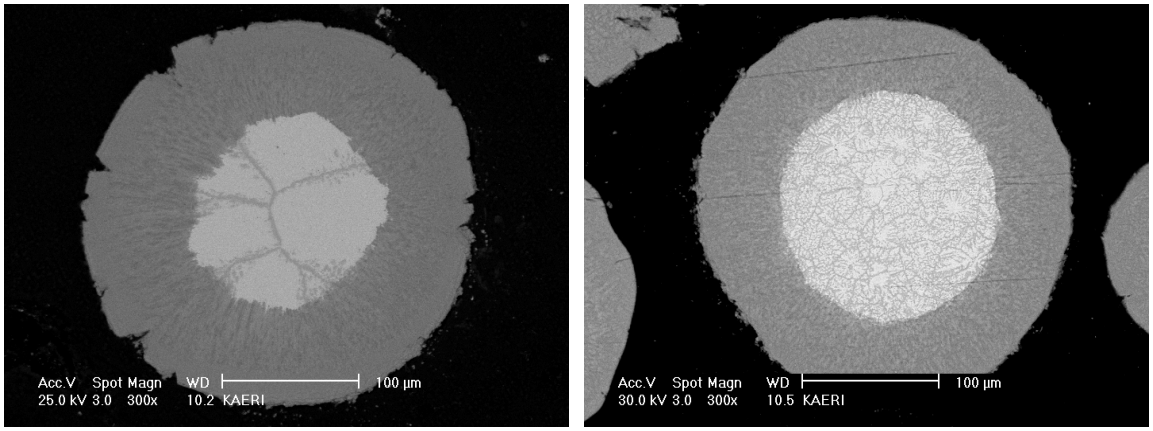

(a) (b)

Fig. 6. SEM images of the dispersion samples after an annealing at 600°C for 3 hr;
(a) U-7Mo/Al-5Si dispersion (b) U-7Mo-4Zr/Al-5Si dispersion.

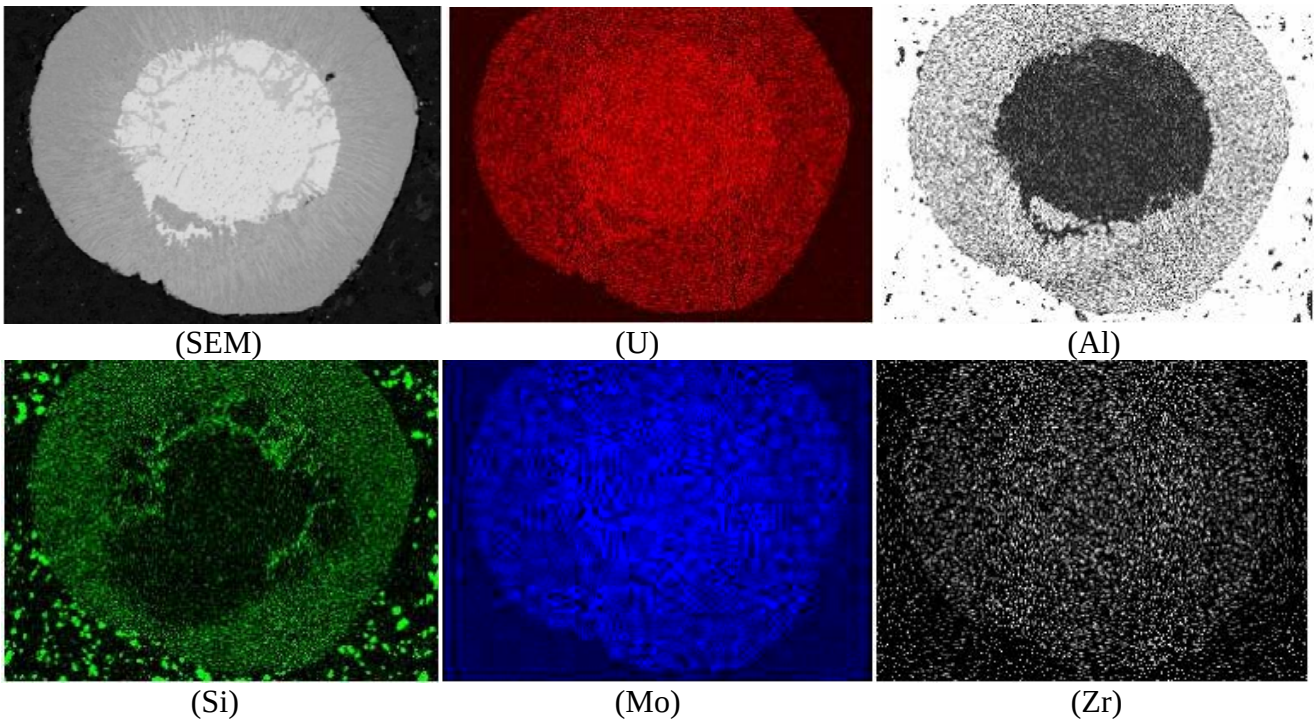

Fig. 7. X-ray element maps of the U-7Mo-2Zr/Al-5Si dispersion fuel sample annealed at 600°C for 3 hr.

Typical interaction product morphologies from the dispersion fuel annealing tests are shown in Fig. 8, in which the interaction product is mostly non-uniform, in other words, modular. The reason for this modular interaction-product growth can be found from the locally inhomogeneous interfacial conditions between the fuel particles and matrix which causes a different reaction rate, locally. For example, some spots have a better contact due to a thinner surface oxide and higher contact pressure than the rest, which results in a faster interaction product growth there than the rest. In Fig.8(b), indeed, we can see discontinuity between the fuel particle and matrix where no interaction product has formed. On the other hand, the contact appears to be good where the interaction product has formed. This type of reaction morphology was more frequently observed for the test samples with larger fuel particles and with Al matrices containing high-Si contents, both of which cause non-uniform contact between the fuel particles and matrix. In this type of interaction product growth, it is very hard to compare the rates. Hence, correlating the growth rates with respect to the test parameters, i.e., temperature, fuel and matrix composition, and time, is meaningless. In this regard, diffusion couple tests are more efficient [14,15].

The IL thickness data of the U-7Mo-xZr vs. Al diffusion couples annealed at 580°C for 5 hr are compared in Fig. 9 for the Zr content in the U-7Mo alloys. The IL thickness between the U-Mo-xZr and Al decreases as the Zr content increases in the U-Mo-xZr. The formation of a multi-phase structure in the IL becomes more notable as the Zr content increases. The diffusion couple U-7Mo-4Zr vs. Al-5Si shows a thinner IL than the diffusion couple U-7Mo-4Zr vs. Al as shown in Fig. 10. The effect of Si in a diffusion couple U-7Mo vs. Al-Si was a negligible reduction in the IL growth rate at 600°C, the effect of Si on an IL thickness reduction seemed to be enhanced when Zr was simultaneously added to U-7Mo. To interpret this result, we hypothesize that the reduction in the IL thickness growth when adding Si and Zr simultaneously is due to an interception of the fast moving atoms, i.e., Si toward U-Mo and Zr toward Al, and forming a high-density product such as $U(Al,Si)_2$ or $U(Al,Si)_3$, which acts like a diffusion barrier. When used alone, however, they themselves undergo a reaction with U-Mo by Si and Al by Zr, resulting in an increase in the growth rate. The background for this reasoning is that the Zr-Si pair has the strongest affinity of all the possible pairs involved in the test.

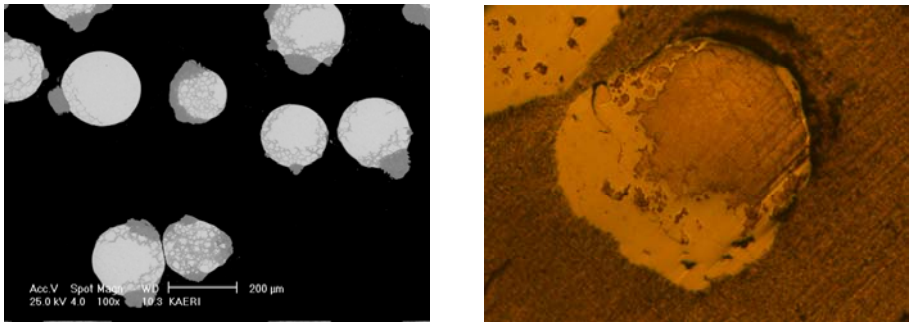

(a) (b)

Fig. 8. (a) SEM image of U-7Mo-4Zr/Al-2Si dispersion fuel and (b) optical image of U-7Mo-4Zr/Al dispersion fuel sample annealed at 550°C for 50 hr.

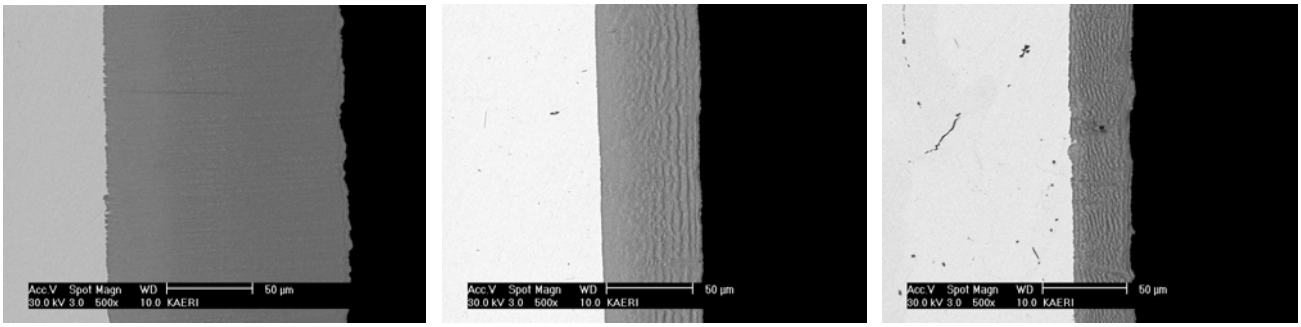

(a) (b) (c)

Fig. 9. SEM images of ILs in (a) U-7Mo vs. Al, (b) U-7Mo-2Zr vs. Al (c) U-7Mo-4Zr vs. Al diffusion couples after an annealing at 580°C for 5 hr.

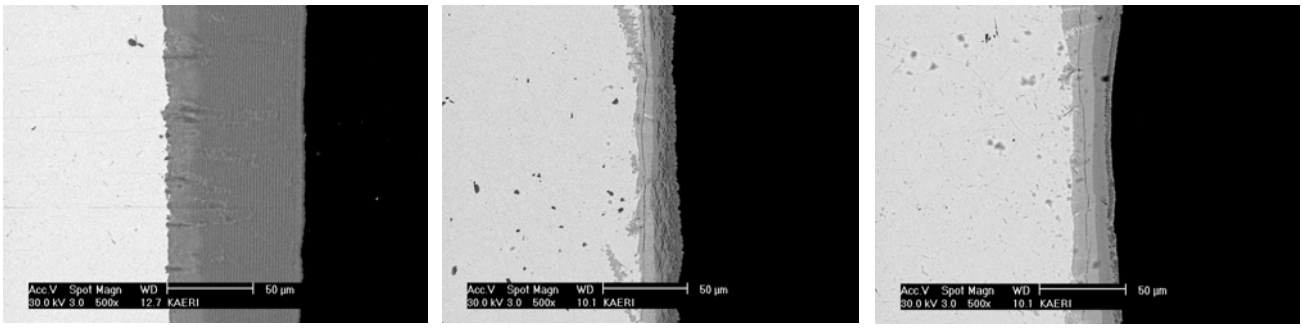

(a) (b) (c)

Fig. 10. SEM images of ILs in (a) U-7Mo-4Zr vs. Al, (b) U-7Mo-4Zr vs. Al-2Si, and (c) U-7Mo-4Zr vs. Al-5Si diffusion couples after an annealing at 600°C for 3 hr.

3-3.Compositional Analysis of IL

We measured the constituent concentrations in the ILs of the diffusion couples by using the EPMA. The concentration distribution profiles are shown in Fig. 11 superimposed on the corresponding micrographs of the interaction products. The U-7Mo vs. Al and U-7Mo-4Zr vs. Al diffusion couples annealed at 600°C for 3 hr exhibited similar profiles for U, Mo, Zr, and Al in the interaction products as in Fig. 11 (a) and (b). The Al-to-U ratio increased from the U-Mo side to the Al side of the interaction products, whereas the Zr-to-U ratio remained constant throughout the interaction products. In the U-7Mo-4Zr vs. Al diffusion couple shown in Fig.11(b), a striated multi-layer-like morphology is visible in the interaction products [16]. Preferential accumulation of Si in the interaction products was observed

when Al-Si was used, regardless of the fuel alloy type, for the diffusion couple tests as demonstrated in Fig. 11(c). This is consistent with other prediction [4] and test results [5,6]. When Zr was added to U-Mo, however, we found a noticeable difference in the Si distribution as shown in Fig. 11(d). A high-Si accumulation was found in the layer on the U-Mo-Zr. The composition of this layer was similar to that of $U(Al,Si)_2$ and this phase was also observed in Ref. 5.

Figure 12 compares the diffusion paths in the U-Mo vs. Al-Si and U-Mo-Zr vs. Al-Si diffusion couples as plotted in the ternary phase diagrams. They are contrastingly different because, contrary to the U-Mo vs. Al-Si diffusion couples forming an Al-rich $U(Al,Si)_3$ layer, the U-Mo-Zr vs. Al-Si diffusion couples formed a Si-rich $U(Al,Si)_2$ layer in contact with the U-Mo-Zr side. Since Zr is the only difference, it can be deduced that Zr facilitates in the formation of the $U(Al,Si)_2$ compound in the diffusion couple. Since interaction compounds with an Al-to-U ratio less than 4 are favored due to their stability during an irradiation [4], this result provides a beneficial sign. The atomic ratios of (Al+Si) to (U+Mo+Zr) are compared in Fig. 13 for all the test cases. In this figure, we can see that, (i) Zr addition to U-Mo alone, i.e., without a Si addition to Al, regardless of the Zr content, cannot reduce the Al-to-(U+Mo+Zr) ratio of the interaction product to below 4. (ii) The combinations that satisfy this requirement are U-7Mo vs. Al-5Si and U-7Mo-2Zr vs. Al-5Si. (iii) The latter case produced the best result.

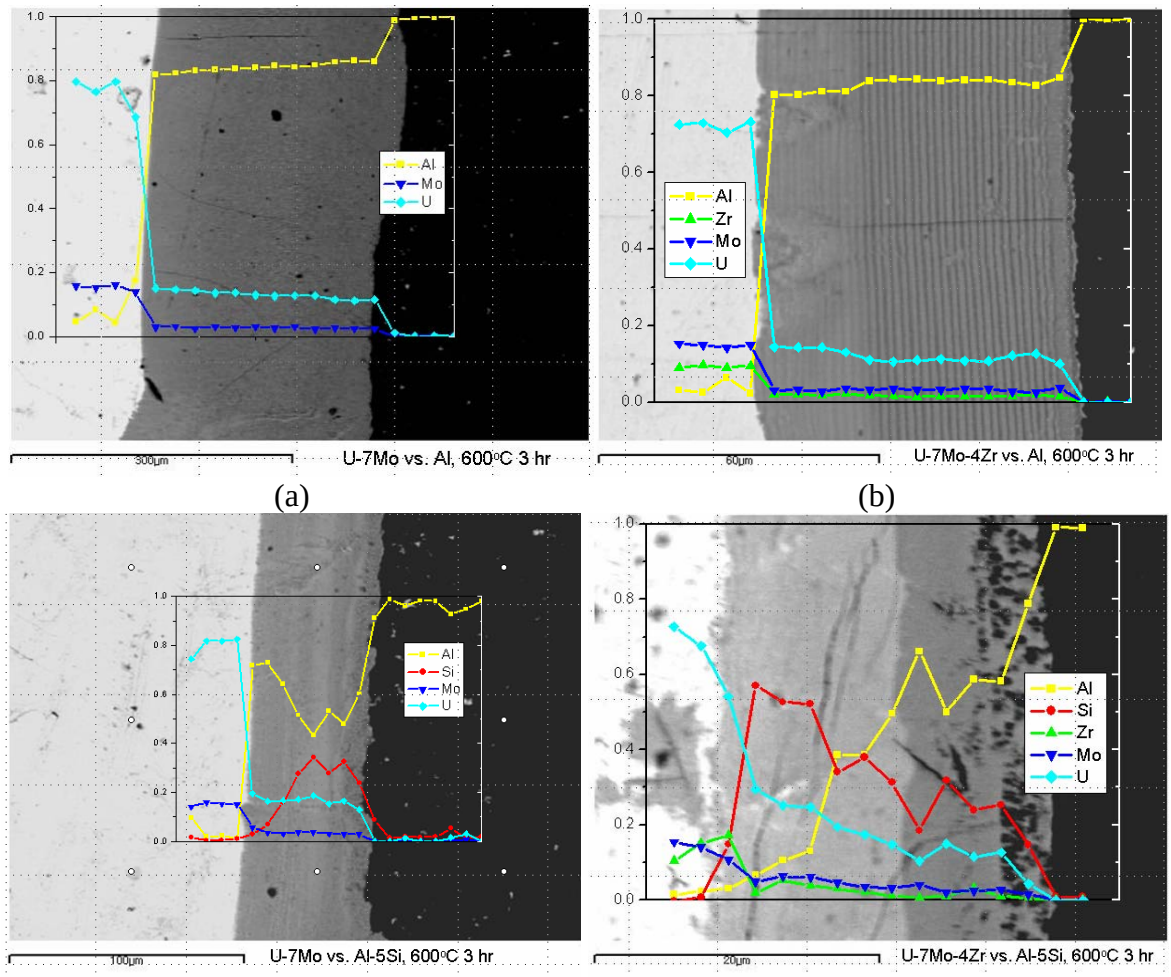

Fig. 11. Compositional profile of IL in (a) U-7Mo vs. Al and (b) U-7Mo-4Zr vs. Al, (c) U-7Mo vs. Al-5Si and (d) U-7Mo-4Zr vs. Al-5Si diffusion couples annealed at 600°C for 3 hr.

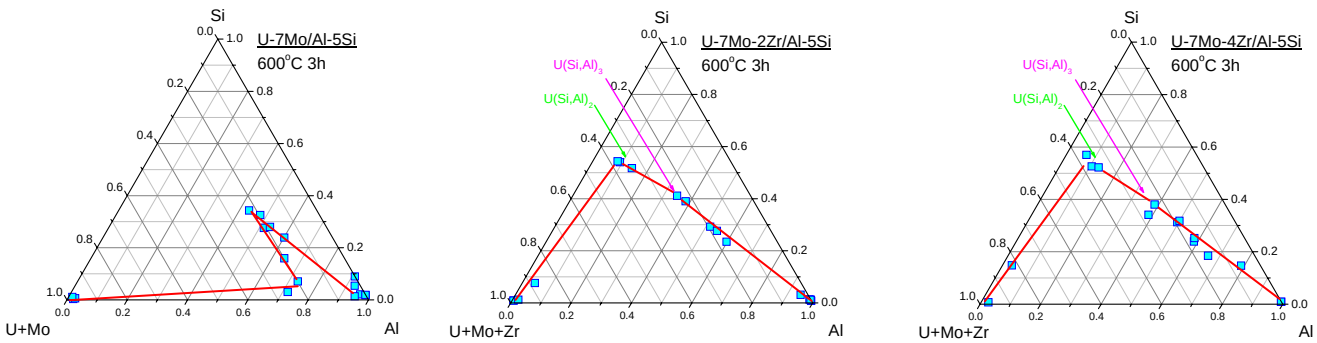

(a) (b) (c)

Fig. 12. Comparison of the diffusion paths for the inter-diffusion of (a) U-7Mo/Al-5Si, (b) U-7Mo-2Zr/Al-5Si, and (c)U-7Mo-4Zr/Al-5Si diffusion couples annealed at 600°C for 3 hr.

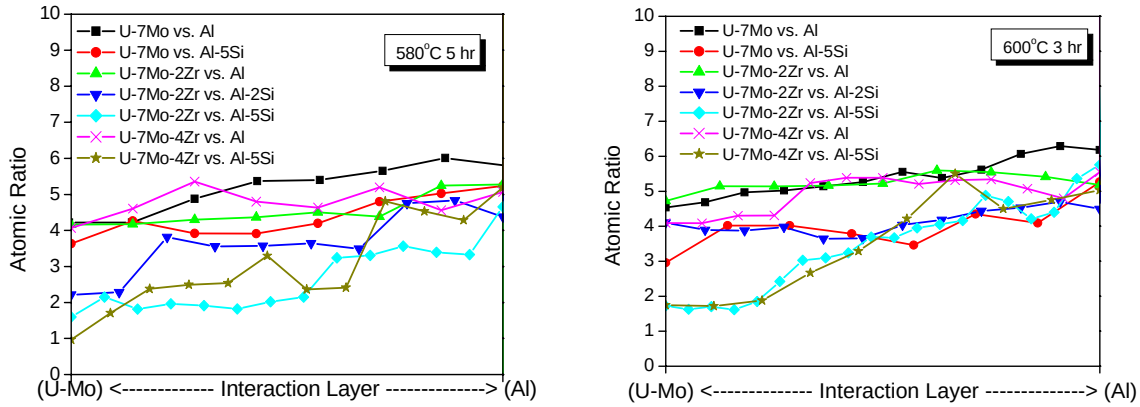

(a) (b)

Fig. 13. Composition ratios of (Al+Si) to (U+Mo+Zr) in the interaction products of the U-7Mo-xZr vs. Al-ySi diffusion couples annealed at (a) 600°C for 3 hr and (b) 580°C 5 hr.

4. Conclusions

From the experimental results and discussions, we can draw the following conclusions:

(1) Zr addition to U-7Mo generally reduced the γ-phase stability of the U-Mo alloy and the rate of γ → α + γ' transformation increased as the Zr content increased beyond 2 wt%.
(2) Diffusion couple tests were a better method to measure the IL thickness than the dispersion sample annealing tests because only the former produced well defined layers to measure whereas the latter produced uneven, modular type interaction products, which were difficult to quantify.
(3) Diffusion couple tests revealed that a Zr addition to U-7wt%Mo reduced the IL growth rates progressively with the Zr content and a Si addition to Al also suppressed the IL growth rates.
(4) Substantial Si accumulation in the ILs was observed when added to Al whereas Zr only accumulate to a minor extent in the ILs when added to U-Mo.
(5) Zr addition to U-Mo alloy worked better when Si was added to Al compared to pure Al. An interaction product with a composition of Si-rich $U(Si,Al)_2$ formed on U-Mo-Zr in a U-Mo-Zr vs. Al-Si diffusion couple.

Acknowledgment

This study was supported as a National Nuclear Research Program by the Ministry of Science and Technology of Korea (MOST).

References

[1] J.L. Snelgrove, G.L. Hofman, M.K. Meyer, C.L. Trybus, T.C. Wiencek, *Nucl. Eng. Des.*, 1997, **178** (1997) 119.
[2] A. Leenaers, S. Van den Berghe, E. Koonen, C. Jarousse, F. Huet, M. Trotabas, M. Boyard, S. Guillot, L. Sannen, M. Verwerft, *J. Nucl. Mater.*, **335** (2004) 39.
[3] L.S. DeLuca and H.T.Sumsion, KAPL-1747, Knolls Atomic Power Labvoratory, (1957).
[4] Y.S. Kim, G.L. Hofman, H.J. Ryu, J. Rest, 27th RERTR International Meeting, Boston, USA, Nov. 6-10, 2005.
[5] M. Mirandou, S. Arico, L. Gribaudo, S. Balart, 27th RERTR International Meeting, Boston, USA, Nov. 6-10, 2005.
[6] J.M.Park, H.J.Ryu, G.G.Lee, H.S.Kim, Y.S.Lee, C.K.Kim, Y.S. Kim, G.L. Hofman, 27th RERTR International Meeting, Boston, USA, Nov. 6-10, 2005.
[7] G.L. Hofman, Y.S. Kim, H.J. Ryu, J. Rest, D. Wachs, M.R. Finlay, 10th International Topical Meeting on RRFM, Sofia, Bulgaria, 2006.
[8] M. Ripert, S. Dubois, P. Boulcourt, S. Naury, P. Lemoine, 10th International Topical Meeting on RRFM, Sofia, Bulgaria, 2006.
[9] C.K. Kim, K.H. KIM, J.M. Park, H.J. Ryu, Y.S. Lee, D.B. Lee, S.J. Oh, H.T. Chae, C.G. Seo, C.S.Lee, 27th RERTR International Meeting, Boston, USA, Nov. 6-10, 2005.
[10] H.E. Exner, G. Petzow, *Metall*, 1969, **23**, p.220-225.
[11] G.L. Hofman, M.K. Meyer, A.E. Ray, 1998 RERTR International Meeting, Sao Paulo, Brazil, Oct. 18-23, 1998.
[12] C.A.W. Peterson et al., UCRL-7824, TID-4500 (34th ed.), Univ. of Calif., National Technical Information Service, US DOC, 1964.
[13] K.H. Kim, H.J. Kwon, J.M. Park, Y.S. Lee, C.K. Kim, *J. Kor. Nucl. Soc.*, 2001, **33** (2001) 365.
[14] H.J. Ryu, Y.S. Han, J.M. Park, S.D. Park, C.K. Kim, *J. Nucl. Mater.*, **321** (2003) 210.
[15] M.I. Mirandou, S.N. Balart, M. Ortiz, M.S. Granovsky, *J. Nucl. Mater.*, **323** (2003) 29.
[16] A.A. Kodentsov, M.R. Rijnders, F.J.J. Van Loo, *Acta Mater.*, **46** (1998) 6521.